estimate of the POS component of the magnetic field. Assuming a typical electron density of 10^8 cm^{-3}, our measured phase speeds between 1.5 and 5 Mm s^{-1} correspond to projected magnetic field strengths between 8 and 26 G. We note that circular polarization measurements of coronal emission lines can provide an estimate of the LOS component of the magnetic field. Notably, seismology and polarimetry provide complementary projections of the coronal magnetic field, which can be combined to provide an estimate of both the strength and the inclination of the magnetic field. In future work, it will be possible to estimate the plasma density with CoMP observations through the intensity ratio of the FeXIII lines at 1074.7 and 1079.8 nm (31).

We have analyzed observations from the CoMP instrument that show an overwhelming flux of upward-propagating low-frequency waves throughout the solar corona. These waves propagate at speeds typical of Alfvén waves, and their direction of propagation mirrors the measured magnetic field direction. The waves we resolved do not have enough energy to heat the solar corona. We conclude that these ubiquitous waves are indeed Alfvénic and offer the real possibility of probing the plasma environment of the solar corona with a high degree of accuracy through coronal seismology.

References and Notes
1. H. Alfvén, *Nature* **150**, 405 (1942).
2. H. Alfvén, *Mon. Not. R. Astron. Soc.* **107**, 211 (1947).
3. D. Osterbrock, *Astrophys. J.* **134**, 347 (1961).
4. M. J. Aschwanden, L. Fletcher, C. J. Schrijver, G. Alexander, *Astrophys. J.* **520**, 880 (1999).
5. V. M. Nakariakov, L. Ofman, E. E. DeLuca, B. Roberts, J. M. Davila, *Science* **285**, 862 (1999).
6. C. E. DeForest, J. B. Gurman, *Astrophys. J.* **501**, L217 (1998).
7. I. De Moortel, J. Ireland, R. W. Walsh, *Astron. Astrophys.* **355**, L23 (2000).
8. M. A. Marsh, R. W. Walsh, *Astrophys. J.* **643**, 540 (2006).
9. M. Minarovjech *et al.*, *Sol. Phys.* **213**, 269 (2003).
10. D. R. Williams *et al.*, *Mon. Not. R. Astron. Soc.* **326**, 428 (2001).
11. J. M. Pasachoff, F. A. Babcock, K. D. Russell, D. B. Seaton, *Sol. Phys.* **207**, 241 (2002).
12. S. Koutchmy, I. D. Zhugzhda, V. Locans, *Astron. Astrophys.* **120**, 185 (1983).
13. T. Sakurai, K. Ichimoto, K. P. Raju, J. Singh, *Sol. Phys.* **209**, 265 (2002).
14. J. W. Belcher, *Astrophys. J.* **168**, 505 (1971).
15. P. Charvin, *Ann. Astrophys.* **28**, 877 (1965).
16. S. M. Jefferies *et al.*, *Astrophys. J.* **434**, 795 (1994).
17. W. Finsterle *et al.*, *Astrophys. J.* **613**, L185 (2004).
18. S. W. McIntosh, B. Fleck, T. D. Tarbell, *Astrophys. J.* **609**, L95 (2004).
19. B. W. Lites, R. Rutten, W. Kalkofen, *Astrophys. J.* **414**, 345 (1993).
20. B. De Pontieu, R. Erdélyi, I. DeMoortel, *Astrophys. J.* **624**, L61 (2005).
21. V. H. Hansteen *et al.*, *Astrophys. J.* **647**, L73 (2006).
22. S. W. McIntosh, S. M. Jefferies, *Astrophys. J.* **647**, L77 (2006).
23. S. M. Jefferies *et al.*, *Astrophys. J.* **648**, L151 (2006).
24. B. De Pontieu *et al.*, *Astrophys. J.* **655**, 624 (2007).
25. O. Wikstol, P. G. Judge, V. Hansteen, *Astrophys. J.* **501**, 895 (1998).
26. P. G. Judge, A. Pietarila, *Astrophys. J.* **606**, 1258 (2004).
27. D. Melrose, *Aust. J. Phys.* **30**, 647 (1977).
28. G. L. Withbroe, R. W. Noyes, *Annu. Rev. Astron. Astrophys.* **15**, 363 (1977).
29. E. Verwichte, C. Foullon, V. M. Nakariakov, *Astron. Astrophys.* **446**, 1139 (2006a).
30. V. M. Nakariakov, E. Verwichte, *Living Rev. Sol. Phys.* **2**, 3 (2005).
31. M. J. Penn *et al.*, *Space Sci. Rev.* **70**, 185 (1994).
32. The authors would like to thank M. Knölker and P. Weis-Taylor for comments on the manuscript. Construction of the CoMP instrument was funded by the NSF through the NCAR Strategic Initiative Fund and HAO/NCAR base funds. The effort of S.M.C. was supported by grant ATM-0541567 from NSF.

Superconducting Interfaces Between Insulating Oxides

N. Reyren,[1] S. Thiel,[2] A. D. Caviglia,[1] L. Fitting Kourkoutis,[3] G. Hammerl,[2] C. Richter,[2] C. W. Schneider,[2] T. Kopp,[2] A.-S. Rüetschi,[1] D. Jaccard,[1] M. Gabay,[4] D. A. Muller,[3] J.-M. Triscone,[1] J. Mannhart[2]*

At interfaces between complex oxides, electronic systems with unusual electronic properties can be generated. We report on superconductivity in the electron gas formed at the interface between two insulating dielectric perovskite oxides, LaAlO$_3$ and SrTiO$_3$. The behavior of the electron gas is that of a two-dimensional superconductor, confined to a thin sheet at the interface. The superconducting transition temperature of $\cong$ 200 millikelvin provides a strict upper limit to the thickness of the superconducting layer of $\cong$ 10 nanometers.

I n pioneering work, it was demonstrated that a highly mobile electron system can be induced at the interface between LaAlO$_3$ and SrTiO$_3$ (1). The discovery of this electron gas at the interface between two insulators has generated an impressive amount of experimental and theoretical work (2–8), in part because the complex ionic structure and particular interactions found at such an interface are expected to promote novel electronic phases that are not always stable as bulk phases (9–11). This result also generated an intense debate on the origin of the conducting layer, which could either be "extrinsic" and due to oxygen vacancies in the SrTiO$_3$ crystal or "intrinsic" and related to the polar nature of the LaAlO$_3$ structure. In the polar scenario, a potential develops as the LaAlO$_3$ layer thickness increases that may lead to an "electronic reconstruction" above some critical thickness (5). Another key issue concerns the ground state of such a system; at low temperatures, a charge-ordered interface with ferromagnetic spin alignment was predicted (4). Experimental evidence in favor of a ferromagnetic ground state was recently found (6). Yet, rather than ordering magnetically, the electron system may also condense into a superconducting state. It was proposed that in field effect transistor configurations, a superconducting, two-dimensional (2D) electron gas might be generated at the SrTiO$_3$ surface (12). It was also pointed out that the polarization of the SrTiO$_3$ layers may cause the electrons on SrTiO$_3$ surfaces to pair and form at high temperatures a superconducting condensate (13, 14). In this report, we explore the ground state of the LaAlO$_3$/SrTiO$_3$ interface and clarify whether it orders when the temperature approaches absolute zero. Our experiments provide evidence that the investigated electron gases condense into a superconducting phase. The characteristics of the transition are consistent with those of a 2D electron system undergoing a Berezinskii-Kosterlitz-Thouless (BKT) transition (15–17). In the oxygen vacancy scenario the observation of superconductivity provides a strict upper limit to the thickness of the superconducting sheet at the LaAlO$_3$/SrTiO$_3$ interface.

The samples were prepared by depositing LaAlO$_3$ layers with thicknesses of 2, 8, and 15 unit cells (uc) on TiO$_2$-terminated (001) surfaces of SrTiO$_3$ single crystals (5, 18). The films were grown by pulsed laser deposition at 770°C and 6×10^{-5} mbar O$_2$, then cooled to room temperature in 400 mbar of O$_2$, with a 1-hour oxidation step at 600°C. The fact that only heterostructures with a LaAlO$_3$ thickness greater than three uc conduct (5) was used to pattern the samples (19). Without exposing the LaAlO$_3$/SrTiO$_3$ interface to the environment, bridges with widths of 100 μm and lengths of 300 μm and 700 μm were structured for four-point measurements, as well as two-uc-thick LaAlO$_3$ layers for reference (18).

[1]Département de Physique de la Matière Condensée, University of Geneva, 24 quai Ernest-Ansermet, 1211 Genève 4, Switzerland. [2]Experimental Physics VI, Center for Electronic Correlations and Magnetism, Institute of Physics, University of Augsburg, D-86135 Augsburg, Germany. [3]School of Applied and Engineering Physics, Cornell University, Ithaca, NY 14853, USA. [4]Laboratoire de Physique des Solides, Bat 510, Université Paris-Sud 11, Centre d'Orsay, 91405 Orsay, Cedex, France.

*To whom correspondence should be addressed. E-mail: jochen.mannhart@physik.uni-augsburg.de

Transmission electron studies (*18*) were performed on reference samples grown under conditions identical to those described above. Cross-sectional cuts were prepared by mechanical polishing followed by low-energy, low-angle ion milling and investigated by scanning transmission electron microscopy (STEM) (*18*). Figure 1A shows a high-angle annular dark field (HAADF) STEM image of the sharp interface between a 15-uc-thick $LaAlO_3$ film and the $SrTiO_3$ substrate. The film is found to be coherent with the substrate with no obvious defects or dislocations at the interface, resulting in biaxial tensile strain of $\cong$ 3%, as measured from ST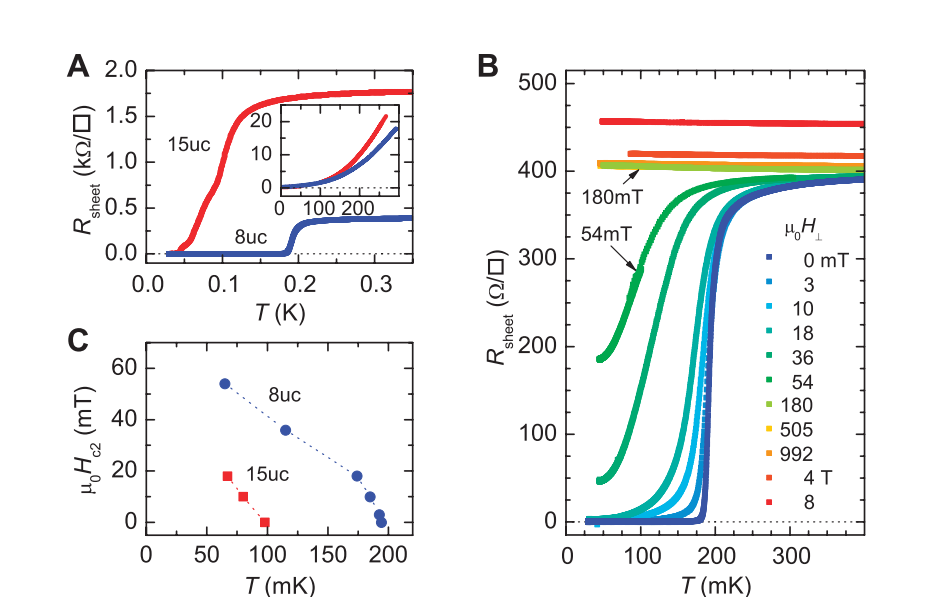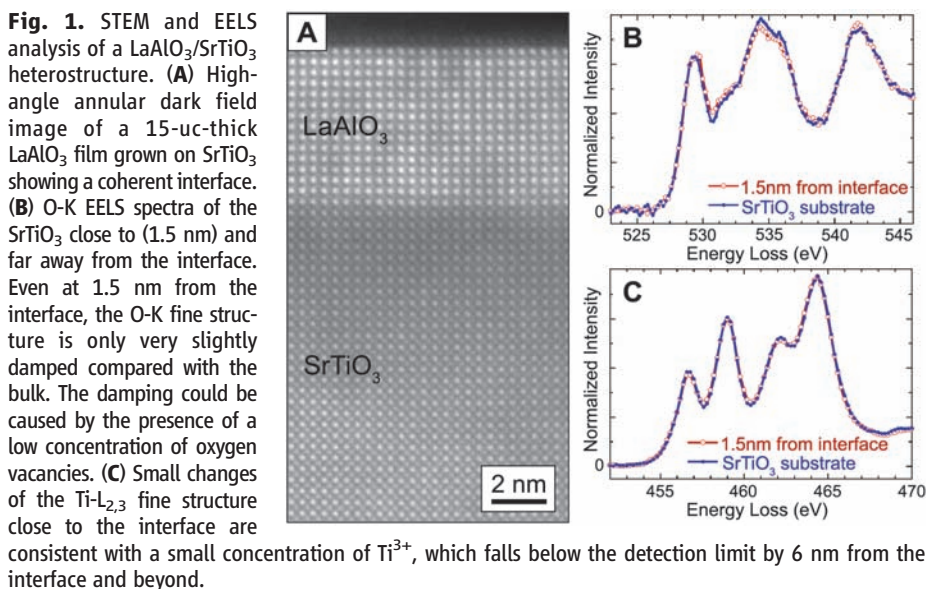EM images (*18*). The out-of-plane lattice constant of the $LaAlO_3$ film is $\cong$ 3.78 Å, which is close to the bulk value and suggests either a rather small Poisson ratio as previously reported (*20*) or out-of-plane relaxation in the thin film (*21*). To obtain an upper limit on the extent of electronic structure and compositional changes below the interface, electron energy-loss spectroscopy (EELS) in the STEM was used to probe the chemistry of the heterostructure at the atomic scale. Simultaneously recorded O-K and $Ti-L_{2,3}$ edges close to and far away from the interface are shown in Fig. 1, B and C. By 1.5 nm away from the interface, the changes in the O-K edge are very slight, suggesting an upper limit to the oxygen vacancy concentration of 3%. At 6 nm away from the interface, the changes in the O-K and $Ti-L_{2,3}$ edges compared with bulk $SrTiO_3$ fall below the noise level (<1% oxygen vacancy concentration). The small changes of the $Ti-L_{2,3}$ edges are consistent with a slight increase in Ti^{3+}, either from oxygen deficiency (*22*) or a compensating interface charge (*18*).

Two samples were analyzed by transport measurements and found to be conducting (Fig. 2A), their 2-uc-thick control structures being insulating (resistance R > 30 MΩ) at all temperatures T (32 mK < T < 300 K). At $T \cong$ 4.2 K, the Hall carrier densities of the 8-uc and 15-uc samples equal $\cong 4 \times 10^{13}/cm^2$ and $\cong 1.5 \times 10^{13}/cm^2$, and the mobilities $\cong$ 350 cm^2/Vs and $\cong$ 1000 cm^2/Vs, respectively. Whether the differences in the sample properties present an intrinsic effect that is caused by the variation of the $LaAlO_3$ thickness remains to be explored. The Hall response is only weakly temperature dependent [Hall resistance R_H(300 K)/R_H(4.2 K) $\cong$ 0.8 and 0.95 for the 8-uc and 15-uc samples, respectively]. Magnetic fields up to $\mu_0 H$ = 8 T were applied to the 8-uc-thick sample, revealing a positive magnetoresistance. The samples investigated here do not show a hysteretic magnetoresistance. No minimum is found in the $R(T)$ characteristics of the 8-uc sample, such as was reported recently for $LaAlO_3$/$SrTiO_3$ samples fabricated under different conditions (*6*). For the 15-uc sample, a shallow minimum in the $R(T)$ curve was observed at 4 K.

At $\cong$ 200 mK and $\cong$ 100 mK, respectively, the 8-uc and 15-uc samples undergo a transition into a state for which no resistance could be measured (Fig. 2A). The widths of the transitions (20% to 80%) of the 8-uc and 15-uc samples are $\cong$ 16 mK and $\cong$ 51 mK, respectively. The resistance drops by more than three orders of magnitude to below the noise limit of the measurement (*18*). Application of a magnetic field $\mu_0 H$ = 180 mT perpendicular to the interface completely suppresses this zero-resistance state (Fig. 2B). Figure 3A displays the voltage versus current (*V-I*) characteristics of a bridge in the 8-uc sample, measured using a dc technique. At low temperatures, the *V-I* characteristics show a well-defined critical current I_c. The occurrence of the zero-resistance state and the characteristic $R(T,H)$ and $V(I,H)$ dependencies provide clear evidence for superconductivity.

The $T_c(H)$ dependence, where T_c is defined as $R(T_c) = 0.5 \times R$(1 K), provides a measure for the upper critical field $H_{c2}(T)$. The $H_{c2}(T)$ curve is shown in Fig. 2C; H_{c2}(0 K) $\cong$ 65 mT and $\cong$ 30 mT for the 8-uc and 15-uc samples, corresponding to coherence lengths ξ(0 K) $\cong$ 70 nm and $\cong$ 105 nm, respectively. Figure 3B shows the temperature dependence of the critical currents per unit width. The maximal values of I_c are 98 μA/cm and 5.6 μA/cm for the 8-uc and 15-uc samples, respectively. A steplike structure in the $V(I)$ curves displayed by the 15-uc sample (not shown) indicates that the low I_c of this sample is caused by inhomogeneities. Just below I_c, the

Fig. 1. STEM and EELS analysis of a $LaAlO_3$/$SrTiO_3$ heterostructure. (**A**) High-angle annular dark field image of a 15-uc-thick $LaAlO_3$ film grown on $SrTiO_3$ showing a coherent interface. (**B**) O-K EELS spectra of the $SrTiO_3$ close to (1.5 nm) and far away from the interface. Even at 1.5 nm from the interface, the O-K fine structure is only very slightly damped compared with the bulk. The damping could be caused by the presence of a low concentration of oxygen vacancies. (**C**) Small changes of the $Ti-L_{2,3}$ fine structure close to the interface are consistent with a small concentration of Ti^{3+}, which falls below the detection limit by 6 nm from the interface and beyond.

Fig. 2. Transport measurements on $LaAlO_3$/$SrTiO_3$ heterostructures. (**A**) Dependence of the sheet resistance on T of the 8-uc and 15-uc samples (measured with a 100-nA bias current). (Inset) Sheet resistance versus temperature measured between 4 K and 300 K. (**B**) Sheet resistance of the 8-uc sample plotted as a function of T for magnetic fields applied perpendicular to the interface. (**C**) Temperature dependence of the upper critical field H_{c2} of the two samples.

samples develop a small voltage drop which is proportional to the current and increases with temperature. As Fig. 4A shows for the 8-uc-thick sample, at 30 mK the associated resistance is at least four orders of magnitude smaller than the normal state resistance. With T increasing from 30 mK to 180 mK, the resistance grows exponentially from $\cong$ 0.1 Ω to 10 Ω. Between 180 mK and T_c, the step at I_c disappears and power-law type $V(I)$ curves are measured.

Is the bulk of the $SrTiO_3$ superconducting or is it only a thin sheet at the interface layer?

How thick is the superconducting layer? If the heterostructures were 2D superconductors, the transition into the superconducting state would be a BKT transition, characterized by a transition temperature T_{BKT} at which vortex-antivortex pairs unbind (23). A simple estimate of T_{BKT}, assuming that the sheet superconducting carrier density equals $4 \times 10^{13}/cm^2$, would suggest that in the samples, the BKT and mean field temperatures almost coincide. However, in case of large vortex fugacity, a high density of vortex-antivortex pairs is thermally generated and an ionic-like

vortex-antivortex crystal is formed (24). For such a system, the melting of this lattice represents the BKT transition, which then occurs at lower temperatures. At the BKT transition, the current-induced Lorentz force causes dislocation-antidislocation pairs to unbind, resulting in a $V \propto I^a$ behavior, with $a(T_{BKT}) = 3$.

The samples indeed show clear signatures of the BKT behavior, such as a $V \propto I^a$ power-law dependence (Fig. 4A). As revealed by Fig. 4B, at $T = 188$ mK, the exponent a approaches 3; this temperature is therefore identified as T_{BKT}. The $V(I,T)$ characteristics (Fig. 4A) are very similar to the results of simulations treating finite-size 2D systems (25). The ohmic regime observed below T_{BKT} at small currents is expected for finite size samples and agrees quantitatively with an analysis (18) based on (24).

In addition, the $R(T)$ characteristics are consistent with a BKT transition, for which, close to T_{BKT}, a $R = R_0 \exp(-bt^{-1/2})$ dependence is expected (26). Here, R_0 and b are material parameters and $t = T/T_{BKT} - 1$. As shown by Fig. 4C, the measured $R(T)$ dependence is consistent with this behavior and yields $T_{BKT} \cong$ 190 mK, in agreement with the result of the a-exponent analysis. The superconducting transition of the samples is therefore consistent with that of a 2D superconducting film. Hence, the superconducting layer is thinner than $\xi \cong 70$ nm.

Analysis of the superconducting transition temperature provides an independent bound on the layer thickness. If the superconductivity were due to oxygen defects in $SrTiO_{3-x}$, a carrier density of $\gtrsim 3 \times 10^{19}/cm^3$ would be required for a T_c of 200 mK (27). The measured sheet carrier densities thus give an upper limit for the thickness of the superconducting sheet of $\cong$ 15 nm. Considering that the carrier concentration of the $SrTiO_{3-x}$ layer cannot be constant but has to conform to a profile following Poisson's equation as treated with consideration to the field-dependent $SrTiO_3$ susceptibility (28), one can set an upper limit for the thickness of the superconducting sheet of $\cong$ 10 nm, a value much smaller than that suggested in (7, 8) for the thickness of the conducting layer in reduced $LaAlO_3/SrTiO_3$ heterostructures. The carrier density profile at interfaces in oxygen-deficient $SrTiO_{3-x}$ has also been calculated in (8). As a result of this model, a sheet carrier density $> 5 \times 10^{14}/cm^2$ is needed to provide a carrier concentration of $3 \times 10^{19}/cm^3$. Because the sheet carrier densities of our samples equal only 1.5 to $4 \times 10^{13}/cm^2$, according to this model the superconductivity of the $LaAlO_3/SrTiO_3$ interface cannot be caused by doped $SrTiO_{3-x}$ alone.

The experiments presented here do not allow us to determine whether the observed superconductivity is due to a thin doped $SrTiO_3$ sheet or a novel phenomenon occurring at this artificial interface. Although the T_c of the heterostructures falls in the transition range of oxygen-deficient $SrTiO_{3-x}$, the transport properties of the samples differ to some extent from the ones of doped
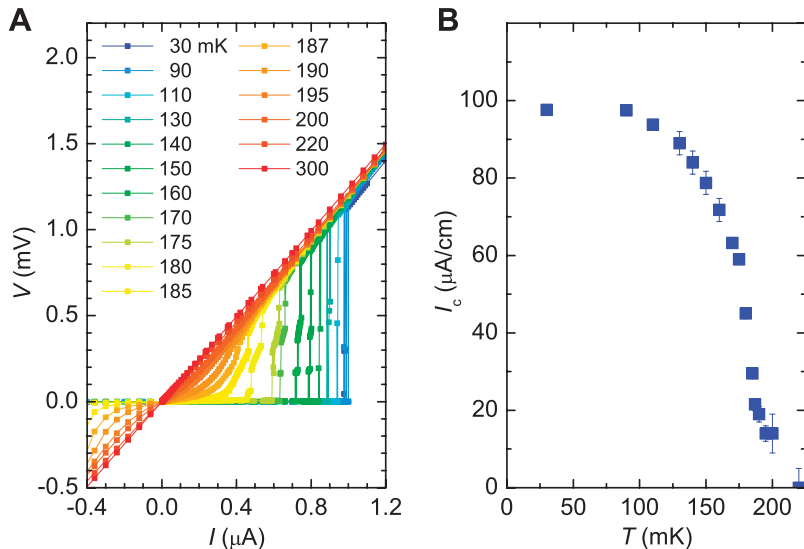
Fig. 3. $V(I)$ measurements of the 8-uc $LaAlO_3/SrTiO_3$ heterostructure. (**A**) Temperature-dependent voltage-current characteristics of a 100×300 μm^2 bridge. (**B**) Measured temperature dependence of the linear critical current density, as obtained from (**A**).
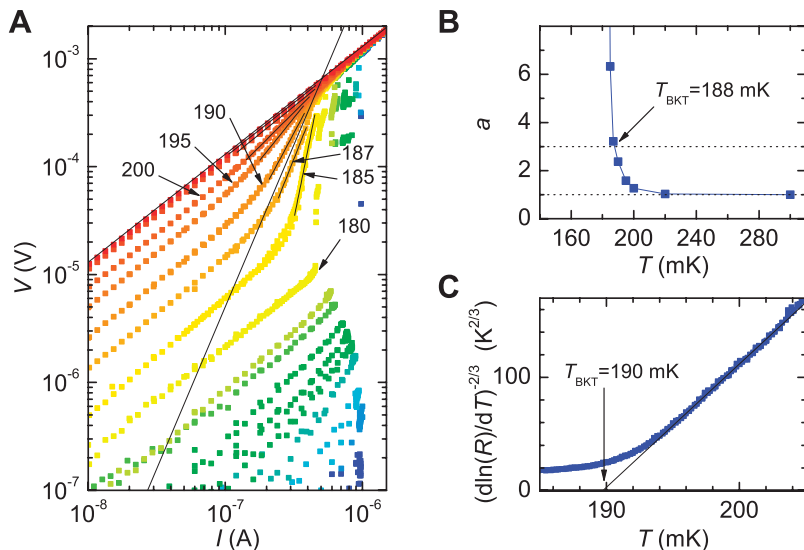
Fig. 4. Low-temperature transport properties of the 8-uc $LaAlO_3/SrTiO_3$ heterostructure. (**A**) $V(I)$ curves on a logarithmic scale. The color code is the same as that in Fig. 3A. The numbers provide the value of T, measured in mK, at which the curves were taken. The short black lines are fits of the data in the transition. The two long black lines correspond to $V = RI$ and $V \sim I^3$ dependencies and show that 187 mK $< T_{BKT} <$ 190 mK. (**B**) Temperature dependence of the power-law exponent a, as deduced from the fits shown in (**A**). (**C**) $R(T)$ dependence of the 8-uc sample ($I = 100$ nA), plotted on a $[d\ln(R)/dT]^{-2/3}$ scale. The solid line is the behavior expected for a BKT transition with $T_{BKT} = 190$ mK.

SrTiO$_3$. Whereas in oxygen-deficient SrTiO$_{3-x}$ and Nb-doped SrTiO$_3$ films the Hall constant increases markedly below 100 K (29), it is less temperature dependent in LaAlO$_3$/SrTiO$_3$ hetero-structures. In addition, the upper critical field of the heterostructures is an order of magnitude smaller than that of Nb-SrTiO$_3$ with the same T_c. Finally, our observation of both superconducting and insulating behavior on the same sample, depending on the precise LaAlO$_3$ layer thickness, is very hard to reconcile with a pure oxygen vacancy scenario.

References and Notes

1. A. Ohtomo, H. Y. Hwang, *Nature* **427**, 423 (2004).
2. N. Nakagawa, H. Y. Hwang, D. A. Muller, *Nat. Mater.* **5**, 204 (2006).
3. M. Huijben *et al.*, *Nat. Mater.* **5**, 556 (2006).
4. R. Pentcheva, W. E. Pickett, *Phys. Rev. B* **74**, 035112 (2006).
5. S. Thiel, G. Hammerl, A. Schmehl, C. W. Schneider, J. Mannhart, *Science* **313**, 1942 (2006).
6. A. Brinkman *et al.*, *Nat. Mater.* **6**, 493 (2007).
7. G. Herranz *et al.*, *Phys. Rev. Lett.* **98**, 216803 (2007).
8. W. Siemons *et al.*, *Phys. Rev. Lett.* **98**, 196802 (2007).
9. S. Altieri, L. H. Tjeng, G. A. Sawatzky, *Thin Solid Films* **9**, 400 (2001).
10. S. Okamoto, J. Millis, *Nature* **428**, 630 (2004).
11. J. Mannhart, in *Thin Films and Heterostructures for Oxide Electronics*, S. Ogale, Ed. (Springer, New York, 2005), pp. 251–278.
12. M. Gurvitch, H. L. Stormer, R. C. Dynes, J. M. Graybeal, D. C. Jacobson, in *Proceedings of the MRS*, J. Bevk, A. I. Braginski, Eds. (Materials Research Society, Warrendale, PA, 1986), pp. 47–49.
13. V. Koerting, Q. Yuan, P. J. Hirschfeld, T. Kopp, J. Mannhart, *Phys. Rev. B* **71**, 104510 (2005).
14. N. Pavlenko, T. Kopp, *Phys. Rev. B* **72**, 174516 (2005).
15. V. L. Berezinskii, *Zh. Eksp. Teor. Fiz.* **61**, 1144 (1971).
16. V. L. Berezinskii, *Sov. Phys. JETP* **34**, 610 (1972).
17. J. M. Kosterlitz, D. J. Thouless, *J. Phys. C* **5**, L124 (1972).
18. Materials and methods are available as supporting material on *Science* Online.
19. C. W. Schneider, S. Thiel, G. Hammerl, C. Richter, J. Mannhart, *Appl. Phys. Lett.* **89**, 122101 (2006).
20. J.-L. Maurice *et al.*, *Phys. Stat. Sol. (A)* **203**, 2209 (2006).
21. M. M. J. Treacy, J. M. Gibson, *J. Vac. Sci. Tech. B* **4**, 1458 (1986).
22. D. A. Muller, N. Nakagawa, A. Ohtomo, J. L. Grazul, H. Y. Hwang, *Nature* **430**, 657 (2004).
23. M. R. Beasley, J. E. Mooij, T. P. Orlando, *Phys. Rev. Lett.* **42**, 1165 (1979).
24. M. Gabay, A. Kapitulnik, *Phys. Rev. Lett.* **71**, 2138 (1993).
25. K. Medvedyeva, B. J. Kim, P. Minnhagen, *Phys. Rev. B* **62**, 14531 (2000).
26. B. I. Halperin, D. R. Nelson, *J. Low Temp.* **36**, 599 (1979).
27. C. S. Koonce, M. L. Cohen, J. F. Schooley, W. R. Hosler, E. R. Pfeiffer, *Phys. Rev.* **163**, 380 (1967).
28. K. Ueno, thesis, University of Tokyo (2003).
29. K. S. Takahashi *et al.*, *Nature* **441**, 195 (2006).
30. The authors acknowledge fruitful discussions and interactions with D. Matthey and D. G. Schlom. This work was supported by the Swiss National Science Foundation through the National Centre of Competence in Research "Materials with Novel Electronic Properties" and the Swiss National Science Foundation Division II, by the Bundesministerium für Bildung und Forschung through Elektronische Korrelationenund Magnetismus (13N6918), by the Deutsche Forschungsgemeinschaft through the Sonderforschungsbereich 484, by the European Union through Nanoxide, by the European Science Foundation through the "Thin Films for Novel Oxide Devices" program, and by the U.S. National Science Foundation.

Large Magnetic Anisotropy of a Single Atomic Spin Embedded in a Surface Molecular Network

Cyrus F. Hirjibehedin,[1] Chiung-Yuan Lin,[1,2] Alexander F. Otte,[1,3] Markus Ternes,[1,4] Christopher P. Lutz,[1] Barbara A. Jones,[1] Andreas J. Heinrich[1]

Magnetic anisotropy allows magnets to maintain their direction of magnetization over time. Using a scanning tunneling microscope to observe spin excitations, we determined the orientation and strength of the anisotropies of individual iron and manganese atoms on a thin layer of copper nitride. The relative intensities of the inelastic tunneling processes are consistent with dipolar interactions, as seen for inelastic neutron scattering. First-principles calculations indicate that the magnetic atoms become incorporated into a polar covalent surface molecular network in the copper nitride. These structures, which provide atom-by-atom accessibility via local probes, have the potential for engineering anisotropies large enough to produce stable magnetization at low temperatures for a single atomic spin.

Magnetic structures with only a few atomic spins, such as single atoms and clusters on metal surfaces (1, 2) and molecular magnets (3–5), can exhibit anisotropies that are large enough to maintain a stable spin orientation at low temperatures. The large anisotropies per each atom in these small clusters are of interest as a possible way to shrink magnetic bits below the size at which domains in current thin-film magnetic materials become unstable at room temperature. The impending approach of this superparamagnetic limit (6) threatens to halt the decades-long trend toward ever higher storage densities in magnetic memory. Besides this technological relevance, atomic-scale magnetic structures are also of great scientific interest because they exhibit intriguing quantum effects (7–9) and have the potential to be harnessed for quantum computing (10, 11). Access to individual magnetic nanostructures by electronic transport measurements is possible with the use of electromigration junctions (12, 13) and local probes (2, 14–18). Whereas nanoscale junction devices may be more readily adapted to practical applications, studies using local probes provide an understanding of the nano-magnet's local environment, the crucial determinant of atomic-scale anisotropy.

Here we describe magnetic nanostructures with large magnetic anisotropy that can be in-dividually constructed, studied, and manipulated with atomic-scale precision. Individual Fe or Mn atoms were placed at the desired locations on a CuN surface by manipulation with a scanning tunneling microscope (STM) tip. Our calculations indicate that the Fe and Mn atoms are embedded into a molecular network of polar covalently bonded Cu and N atoms within the CuN surface. Incorporation into the surface results in substantial charge transfer and distribution of spin polarization away from the magnetic atom and into the molecular network. We found that inelastic excitations of the atomic spin (14, 15) are very prominent in the electron tunneling from an STM tip through the individual magnetic nanostructures. Changes in the spin-excitation energies as a magnetic field was applied along three orthogonal axes directly yielded both the strength and orientation of axial and transverse magnetic anisotropy for a single magnetic atom. The relative intensities of these inelastic excitations are well-described by a spin-transition matrix element that is analogous to that found in inelastic neutron scattering. These nanomagnetic systems combine large magnetic anisotropies with the flexibility that comes from being accessible on a surface by a local probe (2, 14–18) and the potential for control of the magnetic properties previously available only in molecular magnets. This has great promise because, in the absence of transverse anisotropy, the single Fe atom on CuN would have an energy-reversal barrier similar in magnitude to that observed for atomic spins in the most anisotropic configurations in molecular magnets (4) and on metal surfaces (1).

Experiments were conducted with an ultrahigh-vacuum low-temperature STM with a base temperature of 0.5 K. We measured the differential conductance dI/dV using lock-in detection of the

[1]IBM Research Division, Almaden Research Center, San Jose, CA 95120, USA. [2]Center for Probing the Nanoscale, Stanford University, Stanford, CA 94309, USA. [3]Kamerlingh Onnes Laboratorium, Universiteit Leiden, 2300 RA Leiden, Netherlands. [4]Institut de Physique des Nanostructures, École Polytechnique Fédérale de Lausanne, 1015 Lausanne, Switzerland.

*To whom correspondence should be addressed. E-mail: heinrich@almaden.ibm.com